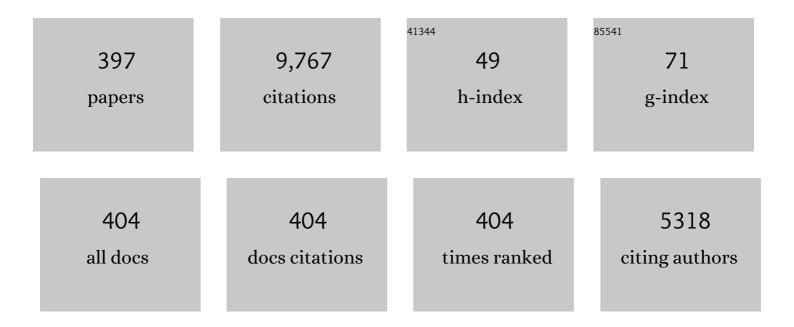
List of Publications by Year in descending order

Source: https://exaly.com/author-pdf/5695584/publications.pdf Version: 2024-02-01



#	Article	IF	CITATIONS
1	An Approach to Obtaining Homogeneously Dispersed Carbon Nanotubes in Al Powders for Preparing Reinforced Al-Matrix Composites. Advanced Materials, 2007, 19, 1128-1132.	21.0	321
2	Enhanced plastic strain in Zr-based bulk amorphous alloys. Physical Review B, 2001, 64, .	3.2	255
3	Effect of aging temperature on microstructure and properties of AlCoCrCuFeNi high-entropy alloy. Intermetallics, 2009, 17, 266-269.	3.9	214
4	Strengthening of nanoprecipitations in an annealed Al0.5CoCrFeNi high entropy alloy. Materials Science & Engineering A: Structural Materials: Properties, Microstructure and Processing, 2016, 671, 82-86.	5.6	158
5	Characterization of hot deformation behavior of a new near beta titanium alloy: Ti-7333. Materials & Design, 2013, 49, 945-952.	5.1	140
6	Deformation and dynamic recrystallization behavior of a high Nb containing TiAl alloy. Journal of Alloys and Compounds, 2013, 552, 363-369.	5.5	120
7	Precipitation behavior of grain boundary M23C6 and its effect on tensile properties of Ni–Cr–W based superalloy. Materials Science & Engineering A: Structural Materials: Properties, Microstructure and Processing, 2012, 548, 83-88.	5.6	119
8	Reducing deformation anisotropy to achieve ultrahigh strength and ductility in Mg at the nanoscale. Proceedings of the National Academy of Sciences of the United States of America, 2013, 110, 13289-13293.	7.1	111
9	Hot deformation mechanism and microstructure evolution of a new near β titanium alloy. Materials Science & Engineering A: Structural Materials: Properties, Microstructure and Processing, 2013, 584, 121-132.	5.6	103
10	Characterization of BCC phases in AlCoCrFeNiTix high entropy alloys. Materials Letters, 2015, 138, 78-80.	2.6	103
11	Enhanced mechanical properties of a CoCrFeNi high entropy alloy by supercooling method. Materials and Design, 2016, 95, 183-187.	7.0	99
12	Dynamic recrystallization and texture evolution of Ti-22Al-25Nb alloy during plane-strain compression. Journal of Alloys and Compounds, 2018, 749, 844-852.	5.5	88
13	Integrating data mining and machine learning to discover high-strength ductile titanium alloys. Acta Materialia, 2021, 202, 211-221.	7.9	85
14	Integrated computational materials engineering for advanced materials: A brief review. Computational Materials Science, 2019, 158, 42-48.	3.0	84
15	The interrelationship of fracture toughness and microstructure in a new near β titanium alloy Ti–7Mo–3Nb–3Cr–3Al. Materials Characterization, 2014, 96, 93-99.	4.4	82
16	Composite structure of α phase in metastable β Ti alloys induced by lattice strain during β to α phase transformation. Acta Materialia, 2017, 132, 307-326.	7.9	80
17	Effect of temperature on tensile behavior of Ni–Cr–W based superalloy. Materials Science & Engineering A: Structural Materials: Properties, Microstructure and Processing, 2011, 528, 1974-1978.	5.6	79
18	Microstructural evolution of a ductile metastable Î ² titanium alloy with combined TRIP/TWIP effects. Journal of Alloys and Compounds, 2017, 699, 775-782.	5.5	76

#	Article	IF	CITATIONS
19	Characterization of hot deformation microstructure of a near beta titanium alloy Ti-5553. Journal of Alloys and Compounds, 2014, 615, 531-537.	5.5	75
20	Characterization of hot deformation behavior of Haynes230 by using processing maps. Journal of Materials Processing Technology, 2009, 209, 4020-4026.	6.3	74
21	Influence of solution treatment on microstructure and mechanical properties of a near β titanium alloy Ti-7333. Materials and Design, 2015, 83, 499-507.	7.0	74
22	Microstructure and properties of bulk Al0.5CoCrFeNi high-entropy alloy by cold rolling and subsequent annealing. Materials Science & Engineering A: Structural Materials: Properties, Microstructure and Processing, 2018, 729, 141-148.	5.6	74
23	High temperature tribological behavior of a Ti-46Al-2Cr-2Nb intermetallics. Intermetallics, 2012, 31, 120-126.	3.9	67
24	Texture evolution and dynamic recrystallization in a beta titanium alloy during hot-rolling process. Journal of Alloys and Compounds, 2015, 618, 146-152.	5.5	67
25	Effect of TiB2 on dry-sliding tribological properties of TiAl intermetallics. Tribology International, 2013, 62, 91-99.	5.9	66
26	Microstructure and mechanical property correlation and property optimization of a near β titanium alloy Ti-7333. Journal of Alloys and Compounds, 2016, 682, 517-524.	5.5	66
27	Hydrogenation thermodynamics of melt-spun magnesium rich Mg–Ni nanocrystalline alloys with the addition of multiwalled carbon nanotubes and TiF3. Journal of Power Sources, 2016, 306, 437-447.	7.8	66
28	Deformation characteristics of as-received Haynes230 nickel base superalloy. Materials Science & Engineering A: Structural Materials: Properties, Microstructure and Processing, 2008, 497, 283-289.	5.6	65
29	Deformation behavior of hot-rolled IN718 superalloy under plane strain compression at elevated temperature. Materials Science & amp; Engineering A: Structural Materials: Properties, Microstructure and Processing, 2014, 606, 24-30.	5.6	65
30	Flow characteristics and constitutive modeling for elevated temperature deformation of a high Nb containing TiAl alloy. Intermetallics, 2014, 49, 23-28.	3.9	65
31	The effect of M23C6 carbides on the formation of grain boundary serrations in a wrought Ni-based superalloy. Materials Science & Engineering A: Structural Materials: Properties, Microstructure and Processing, 2012, 536, 37-44.	5.6	64
32	Atomic and electronic basis for the serrations of refractory high-entropy alloys. Npj Computational Materials, 2017, 3, .	8.7	64
33	Hot forging design and microstructure evolution of a high Nb containing TiAl alloy. Intermetallics, 2015, 58, 7-14.	3.9	62
34	Microstructure control of Ti 45Al 8.5Nb (W, B, Y) alloy during the solidification process. Acta Materialia, 2016, 112, 121-131.	7.9	62
35	The characteristics of serration in Al0.5CoCrFeNi high entropy alloy. Materials Science & Engineering A: Structural Materials: Properties, Microstructure and Processing, 2017, 702, 96-103.	5.6	62
36	Microstructure and hydrogen storage properties of Mg-Ni-Ce alloys with a long-period stacking ordered phase. Journal of Power Sources, 2017, 338, 91-102.	7.8	62

#	Article	IF	CITATIONS
37	Mg–Gd–Y system phase diagram calculation and experimental clarification. Journal of Alloys and Compounds, 2008, 450, 446-451.	5.5	61
38	Effect of thermal exposure on the stability of carbides in Ni–Cr–W based superalloy. Materials Science & Engineering A: Structural Materials: Properties, Microstructure and Processing, 2011, 528, 2339-2344.	5.6	61
39	Tribological Behavior of AlCoCrFeNi(Ti0.5) High Entropy Alloys under Oil and MACs Lubrication. Journal of Materials Science and Technology, 2016, 32, 470-476.	10.7	61
40	The FCC to BCC phase transformation kinetics in an Al0.5CoCrFeNi high entropy alloy. Journal of Alloys and Compounds, 2017, 710, 144-150.	5.5	59
41	Effect of strain rate on compressive behavior of Ti-based bulk metallic glass at room temperature. Journal of Alloys and Compounds, 2009, 472, 214-218.	5.5	57
42	Mechanical properties of porous titanium with different distributions of pore size. Transactions of Nonferrous Metals Society of China, 2013, 23, 2317-2322.	4.2	57
43	Microstructure and mechanical properties of non-equilibrium solidified CoCrFeNi high entropy alloy. Materials Chemistry and Physics, 2018, 210, 192-196.	4.0	57
44	Interfacial in-situ Al2O3 nanoparticles enhance load transfer in carbon nanotube (CNT)-reinforced aluminum matrix composites. Journal of Alloys and Compounds, 2019, 789, 25-29.	5.5	57
45	Understanding the role of carbon atoms on microstructure and phase transformation of high Nb containing TiAl alloys. Materials Characterization, 2017, 124, 1-7.	4.4	55
46	Tensile properties and fracture behavior of in-situ synthesized Ti 2 AlN/Ti48Al2Cr2Nb composites at room and elevated temperatures. Materials Science & Engineering A: Structural Materials: Properties, Microstructure and Processing, 2017, 679, 7-13.	5.6	55
47	A multivariate relationship for the impact sensitivities of energetic N-nitrocompounds based on bond dissociation energy. Journal of Hazardous Materials, 2010, 174, 728-733.	12.4	53
48	Evolution of the secondary α phase morphologies during isothermal heat treatment in Ti-7333 alloy. Journal of Alloys and Compounds, 2013, 577, 516-522.	5.5	53
49	Hydrogen desorption performance of high-energy ball milled Mg 2 NiH 4 catalyzed by multi-walled carbon nanotubes coupling with TiF 3. International Journal of Hydrogen Energy, 2014, 39, 19672-19681.	7.1	51
50	Nanophase precipitation and strengthening in a dual-phase Al0.5CoCrFeNi high-entropy alloy. Journal of Materials Science and Technology, 2021, 72, 1-7.	10.7	51
51	Microstructure and Tribological Properties of AlCoCrFeNiTi0.5 High-Entropy Alloy in Hydrogen Peroxide Solution. Metallurgical and Materials Transactions A: Physical Metallurgy and Materials Science, 2014, 45, 201-207.	2.2	49
52	Microstructure and abrasive wear characteristics of in situ vanadium carbide particulate-reinforced iron matrix composites. Materials & Design, 2014, 54, 564-569.	5.1	49
53	Phase transformation in TC21 alloy during continuous heating. Journal of Alloys and Compounds, 2009, 472, 252-256.	5.5	48
54	Experiments and crystal plasticity finite element simulations of nanoindentation on Ti–6Al–4V alloy. Materials Science & Engineering A: Structural Materials: Properties, Microstructure and Processing, 2015, 625, 28-35.	5.6	47

#	Article	IF	CITATIONS
55	Grain refinement of superalloy K4169 by addition of refiners: cast structure and refinement mechanisms. Materials Science & Engineering A: Structural Materials: Properties, Microstructure and Processing, 2005, 394, 1-8.	5.6	46
56	An experimental study on the mechanism of texture evolution during hot-rolling process in a Î ² titanium alloy. Journal of Alloys and Compounds, 2014, 603, 23-27.	5.5	46
57	Local lattice distortion mediated formation of stacking faults in Mg alloys. Acta Materialia, 2019, 170, 231-239.	7.9	45
58	Diffusion Research in BCC Ti-Al-Mo Ternary Alloys. Metallurgical and Materials Transactions A: Physical Metallurgy and Materials Science, 2014, 45, 1647-1652.	2.2	44
59	Superplastic deformation mechanisms of high Nb containing TiAl alloy with (α2Â+Âγ) microstructure. Intermetallics, 2016, 75, 62-71.	3.9	44
60	A quantitative relationship for the shock sensitivities of energetic compounds based on X–NO2 (X=C,) Tj ETQo	0 0 0 rgB 12.4	T /Qyerlock 1
61	Microstructure and hydrogenation thermokinetics of ZrTi0.2V1.8 alloy. International Journal of Hydrogen Energy, 2010, 35, 11981-11985.	7.1	43
62	Hydrogen absorption properties of Zr(V1â^'xFex)2 intermetallic compounds. International Journal of Hydrogen Energy, 2012, 37, 2328-2335.	7.1	42
63	Dependence of mechanical properties on the microstructure characteristics of a near β titanium alloy Ti-7333. Journal of Materials Science and Technology, 2019, 35, 48-54.	10.7	41
64	Improved tensile properties of Al0.5CoCrFeNi high-entropy alloy by tailoring microstructures. Rare Metals, 2021, 40, 1-6.	7.1	41
65	Static recrystallization simulations by coupling cellular automata and crystal plasticity finite element method using a physically based model for nucleation. Journal of Materials Science, 2014, 49, 3253-3267.	3.7	40
66	De/hydrogenation kinetics against air exposure and microstructure evolution during hydrogen absorption/desorption of Mg-Ni-Ce alloys. Renewable Energy, 2017, 113, 1399-1407.	8.9	40
67	Microstructural characteristics and dynamic recrystallization behavior of β-γ TiAl based alloy during high temperature deformation. Intermetallics, 2018, 97, 52-57.	3.9	40
68	Atomic and electronic basis for solutes strengthened (010) anti-phase boundary of L12 Co3(Al, TM): A comprehensive first-principles study. Acta Materialia, 2018, 145, 30-40.	7.9	40
69	Tribological behavior of AlCoCrCuFeNi and AlCoCrFeNiTi0.5 high entropy alloys under hydrogen peroxide solution against different counterparts. Tribology International, 2015, 92, 203-210.	5.9	39
70	Cellular automata modeling of static recrystallization based on the curvature driven subgrain growth mechanism. Journal of Materials Science, 2013, 48, 7142-7152.	3.7	37
71	Influence of nitrogen on the microstructure and solidification behavior of high Nb containing TiAl alloys. Materials and Design, 2016, 103, 100-105.	7.0	37
72	Characterization of the elevated temperature compressive deformation behavior of high Nb containing TiAl alloys with two microstructures. Materials Science & Engineering A: Structural Materials: Properties, Microstructure and Processing, 2018, 725, 466-478.	5.6	37

#	Article	IF	CITATIONS
73	Hot working characteristic of as-cast and homogenized Ni–Cr–W superalloy. Materials Science & Engineering A: Structural Materials: Properties, Microstructure and Processing, 2009, 508, 141-147.	5.6	36
74	On the poisoning effect of O2 and N2 for the Zr0.9Ti0.1V2 hydrogen storage alloy. Journal of Power Sources, 2012, 202, 217-224.	7.8	36
75	Microstructure and hydrogen storage properties of non-stoichiometric Zr–Ti–V Laves phase alloys. International Journal of Hydrogen Energy, 2013, 38, 14675-14684.	7.1	36
76	Microstructure and tailoring hydrogenation performance of Y-doped Mg2Ni alloys. Journal of Power Sources, 2014, 245, 808-815.	7.8	36
77	Study on the formation mechanism of α lamellae in a near β titanium alloy. Progress in Natural Science: Materials International, 2016, 26, 385-390.	4.4	36
78	Microstructural evolution and FCC twinning behavior during hot deformation of high temperature titanium alloy Ti65. Journal of Materials Science and Technology, 2020, 49, 56-69.	10.7	36
79	Influence of solution temperature on phase transformation of TC21 alloy. Materials Science & Engineering A: Structural Materials: Properties, Microstructure and Processing, 2009, 508, 76-82.	5.6	35
80	Crystallization kinetics of Cu38Zr46Ag8Al8 bulk metallic glass in different heating conditions. Journal of Non-Crystalline Solids, 2014, 404, 7-12.	3.1	35
81	Mechanical properties and pore structure deformation behaviour of biomedical porous titanium. Transactions of Nonferrous Metals Society of China, 2015, 25, 1543-1550.	4.2	35
82	Characteristics of a hot-rolled near Î ² titanium alloy Ti-7333. Materials Characterization, 2017, 129, 135-142.	4.4	35
83	Microstructure evolution and mechanical properties of diffusion bonding high Nb containing TiAl alloy to Ti2AlNb alloy. Vacuum, 2019, 164, 140-148.	3.5	34
84	Effect of strong magnetic field on the microstructure and mechanical-magnetic properties of AlCoCrFeNi high-entropy alloy. Journal of Alloys and Compounds, 2020, 820, 153407.	5.5	34
85	Hydrogenation thermokinetics and activation behavior of non-stoichiometric Zr-based Laves alloys with enhanced hydrogen storage capacity. Journal of Alloys and Compounds, 2017, 694, 300-308.	5.5	33
86	ω-Assisted refinement of α phase and its effect on the tensile properties of a near β titanium alloy. Journal of Materials Science and Technology, 2020, 44, 24-30.	10.7	33
87	Precipitation of α phase and its morphological evolution during continuous heating in a near β titanium alloy Ti-7333. Materials Characterization, 2017, 132, 199-204.	4.4	32
88	Correlation between imposed deformation and transformation lattice strain on α variant selection in a metastable β-Ti alloy under isothermal compression. Acta Materialia, 2018, 161, 150-160.	7.9	32
89	Corrosive and tribological behaviors of AlCoCrFeNi-M high entropy alloys under 90â€⁻wt. % H2O2 solution. Tribology International, 2019, 131, 24-32.	5.9	32
90	Phase precipitation behavior during isothermal deformation in β-quenched near beta titanium alloy Ti-7333. Journal of Alloys and Compounds, 2016, 671, 381-388.	5.5	31

#	Article	IF	CITATIONS
91	Diffusional mobility for fcc phase of Al–Mg–Zn system and its applications. Calphad: Computer Coupling of Phase Diagrams and Thermochemistry, 2008, 32, 602-607.	1.6	30
92	Microstructure and texture of commercially pure titanium in cold deep drawing. Transactions of Nonferrous Metals Society of China, 2012, 22, 496-502.	4.2	30
93	Elements segregation and phase precipitation behavior at grain boundary in a Ni-Cr-W based superalloy. Materials Characterization, 2016, 122, 189-196.	4.4	30
94	Liquid-phase separation in undercooled CoCrCuFeNi high entropy alloy. Intermetallics, 2017, 86, 110-115.	3.9	30
95	Crystallography and asymmetry of tensile and compressive stress-induced martensitic transformation in metastable βÂtitaniumÂalloy Ti–7Mo–3Nb–3Cr–3Al. Journal of Alloys and Compounds, 2019, 809, 15	1762.	30
96	Microstructure and electrochemical hydrogenation/dehydrogenation performance of melt-spun La-doped Mg2Ni alloys. Materials Characterization, 2015, 106, 163-174.	4.4	29
97	Strong work-hardening behavior induced by the solid solution strengthening of dendrites in TiZr-based bulk metallic glass matrix composites. Journal of Alloys and Compounds, 2015, 624, 9-16.	5.5	29
98	Grain boundary character correlated carbide precipitation and mechanical properties of Ni-20Cr-18W-1Mo superalloy. Materials Science & Engineering A: Structural Materials: Properties, Microstructure and Processing, 2016, 667, 391-401.	5.6	29
99	Phase transformation mechanisms in a quenched Ti-45Al-8.5Nb-0.2W-0.2B-0.02YÂalloy after subsequentÂannealingÂatÂ800°C. Journal of Alloys and Compounds, 2017, 691, 60-66.	5.5	29
100	Revealing the local lattice strains and strengthening mechanisms of Ti alloys. Computational Materials Science, 2018, 152, 169-177.	3.0	29
101	Homogeneous deformation of Ti41.5Cu37.5Ni7.5Zr2.5Hf5Sn5Si1 bulk metallic glass in the supercooled liquid region. Intermetallics, 2011, 19, 48-53.	3.9	28
102	Tribological properties of Ti40Zr25Ni8Cu9Be18 bulk metallic glasses under different conditions. Materials & Design, 2011, 32, 4573-4579.	5.1	28
103	Kinetics of the ω phase transformation of Ti-7333 titanium alloy during continuous heating. Journal of Materials Science, 2013, 48, 1966-1972.	3.7	28
104	Computational study of atomic mobility for bcc phase in Ti–Al–Fe system. Calphad: Computer Coupling of Phase Diagrams and Thermochemistry, 2014, 46, 205-212.	1.6	28
105	Strain-rate-dependent deformation behavior in a Ti-based bulk metallic glass composite upon dynamic deformation. Journal of Alloys and Compounds, 2015, 639, 131-138.	5.5	28
106	Hot deformation behavior originated from dislocation activity and \hat{I}^2 to \hat{I}_{\pm} phase transformation in a metastable \hat{I}^2 titanium alloy. International Journal of Plasticity, 2019, 119, 200-214.	8.8	28
107	Synthesis of 3 or 3,3′-substituted BINOL ligands and their application in the asymmetric addition of diethylzinc to aromatic aldehydes. Tetrahedron: Asymmetry, 2005, 16, 3667-3671.	1.8	27
108	Assessment of Atomic Mobilities for bcc Phase of Ti-Al-V System. Journal of Phase Equilibria and Diffusion, 2010, 31, 135-143.	1.4	27

#	Article	IF	CITATIONS
109	Non-isothermal phase transformation kinetics of ω phase in TB-13 titanium alloys. Materials Science & Engineering A: Structural Materials: Properties, Microstructure and Processing, 2010, 527, 5100-5104.	5.6	27
110	Kinetics of orthorhombic martensite decomposition in TC21 alloy under isothermal conditions. Journal of Materials Science, 2012, 47, 521-529.	3.7	27
111	Role of Ni addition on hydrogen storage characteristics of ZrV2 Laves phase compounds. International Journal of Hydrogen Energy, 2016, 41, 10391-10404.	7.1	27
112	Liquid–liquid structure transition and nucleation in undercooled Co-B eutectic alloys. Applied Physics A: Materials Science and Processing, 2017, 123, 1.	2.3	27
113	Texture evolution and the recrystallization behavior in a near β titanium alloy Ti-7333 during the hot-rolling process. Materials Characterization, 2020, 159, 109999.	4.4	27
114	Assessment of diffusion mobility for the bcc phase of the Ti–Al–Cr system. Calphad: Computer Coupling of Phase Diagrams and Thermochemistry, 2011, 35, 384-390.	1.6	26
115	Deformation behavior of a Ti-based bulk metallic glass composite with excellent cryogenic mechanical properties. Materials & Design, 2014, 53, 737-740.	5.1	26
116	Hot Deformation Behavior of As-Cast and Homogenized Al0.5CoCrFeNi High Entropy Alloys. Metals, 2016, 6, 277.	2.3	26
117	Role of milling time and Ni content on dehydrogenation behavior of MgH 2 /Ni composite. Transactions of Nonferrous Metals Society of China, 2017, 27, 569-577.	4.2	26
118	Effect of β/B2 phase on cavitation behavior during superplastic deformation of TiAl alloys. Journal of Alloys and Compounds, 2017, 693, 749-759.	5.5	26
119	Dynamic recrystallization behavior of the Ti–48Al–2Cr–2Nb alloy during isothermal hot deformation. Progress in Natural Science: Materials International, 2019, 29, 587-594.	4.4	26
120	Compressive deformation behaviors of tungsten fiber reinforced Zr-based metallic glass composites. Materials Science & Engineering A: Structural Materials: Properties, Microstructure and Processing, 2008, 486, 308-312.	5.6	25
121	Role of defect structure on hydrogenation properties of Zr0.9Ti0.1V2 alloy. International Journal of Hydrogen Energy, 2011, 36, 9318-9323.	7.1	25
122	Tribological behavior of CNTs-Cu and graphite-Cu composites with electric current. Transactions of Nonferrous Metals Society of China, 2012, 22, 78-84.	4.2	25
123	Hydrogen storage properties of non-stoichiometric Zr0.9Ti V2 melt-spun ribbons. Energy, 2016, 114, 1147-1154.	8.8	25
124	Precipitation behavior of \hat{I}_{\pm} phase during aging treatment in a \hat{I}^2 -quenched Ti-7333. Materials Characterization, 2018, 140, 275-280.	4.4	25
125	Evolution of microstructure and hardness in a dual-phase Al0.5CoCrFeNi high-entropy alloy with different grain sizes. Rare Metals, 2020, 39, 156-161.	7.1	25
126	Enhanced hydrogen absorption kinetics by introducing fine eutectic and long-period stacking ordered structure in ternary eutectic Mg–Ni–Y alloy. Journal of Alloys and Compounds, 2020, 820, 153187.	5.5	25

#	Article	IF	CITATIONS
127	Enhancing mechanical properties of Al0.25CoCrFeNi high-entropy alloy via cold rolling and subsequent annealing. Journal of Alloys and Compounds, 2020, 830, 154645.	5.5	25
128	Effects of Ti and Cu on the Microstructure Evolution of AlCoCrFeNi High-Entropy Alloy During Heat Treatment. Acta Metallurgica Sinica (English Letters), 2020, 33, 1077-1090.	2.9	25
129	Deformation and recrystallization textures in straight-rolled and pseudo cross-rolled AA 3105 aluminum alloy. Journal of Alloys and Compounds, 2010, 491, 301-307.	5.5	24
130	On the amorphization behavior and hydrogenation performance of high-energy ball-milled Mg2Ni alloys. Materials Characterization, 2013, 80, 21-27.	4.4	24
131	General features of high temperature deformation kinetics for Î ³ -TiAl-based alloys with DP/NG microstructures: Part I. A survey of mechanical data and development of unified rate-equations. Materials Science & amp; Engineering A: Structural Materials: Properties, Microstructure and Processing, 2016, 678, 389-401.	5.6	24
132	Fully Recrystallized Al0.5CoCrFeNi High-Entropy Alloy Strengthened by Nanoscale Precipitates. Metals and Materials International, 2019, 25, 1145-1150.	3.4	24
133	Influence of high magnetic field on the liquid-liquid phase separation behavior of an undercooled Cu–Co immiscible alloy. Journal of Alloys and Compounds, 2020, 842, 155502.	5.5	24
134	The microstructures and superconducting properties of MgB2 bulks prepared by a high-energy milling method. Physica C: Superconductivity and Its Applications, 2007, 467, 38-42.	1.2	23
135	Precipitation behavior and strengthening-toughening mechanism of hot rolled sheet of Ti65 titanium alloy during aging process. Journal of Alloys and Compounds, 2020, 831, 154786.	5.5	23
136	Anab initio study of intermolecular interactions of nitromethane dimer and nitromethane trimer. Journal of Computational Chemistry, 2003, 24, 345-352.	3.3	22
137	Synthesis and application of 3â€substituted (<i>S</i>)â€BINOL as chiral ligands for the asymmetric ethylation of aldehydes. Chirality, 2010, 22, 820-826.	2.6	22
138	Electrochemical corrosion properties of Zr- and Ti-based bulk metallic glasses. Transactions of Nonferrous Metals Society of China, 2011, 21, 552-557.	4.2	22
139	Effect of electrical current on tribological property of Cu matrix composite reinforced by carbon nanotubes. Transactions of Nonferrous Metals Society of China, 2011, 21, 2237-2241.	4.2	22
140	Stress induced deformation in the solidification of undercooled Co80Pd20 alloys. Materials Science & Engineering A: Structural Materials: Properties, Microstructure and Processing, 2011, 528, 973-977.	5.6	22
141	β phase transformation kinetics in Ti60 alloy during continuous cooling. Journal of Alloys and Compounds, 2013, 576, 108-113.	5.5	22
142	Characteristics of metadynamic recrystallization of a high Nb containing TiAl alloy. Materials Letters, 2013, 92, 430-432.	2.6	22
143	Microstructural characterization and hydrogenation properties of non-stoichiometric Zr 0.9 Ti x V 2 alloys. International Journal of Hydrogen Energy, 2014, 39, 19637-19645.	7.1	22
144	A mixture of massive and feathery microstructures of Ti48Al2Cr2Nb alloy by high undercooled solidification. Materials Characterization, 2015, 100, 104-107.	4.4	22

#	Article	IF	CITATIONS
145	Nano-precipitation and tensile properties of Ti60 alloy after exposure at 550°C and 650°C. Materials Science & Engineering A: Structural Materials: Properties, Microstructure and Processing, 2015, 626, 247-253.	5.6	22
146	Temperature dependent deformation mechanisms of Al0.3CoCrFeNi high-entropy alloy, starting from serrated flow behavior. Journal of Alloys and Compounds, 2018, 757, 39-43.	5.5	22
147	Formation of slip bands and microstructure evolution of Ti-5Al-5Mo-5V-3Cr-0.5Fe alloy during warm deformation process. Journal of Alloys and Compounds, 2019, 770, 183-193.	5.5	22
148	Nucleation of supercooled Co melts under a high magnetic field. Materials Chemistry and Physics, 2019, 225, 133-136.	4.0	22
149	Electromagnetic shaping and solidification control of Ni-base superalloys under vacuum. Journal of Materials Processing Technology, 2004, 148, 25-29.	6.3	21
150	Effects of alloy addition on the improvement of glass forming ability and plasticity of Mg–Cu–Tb bulk metallic glass. Intermetallics, 2009, 17, 253-255.	3.9	21
151	A phase-field approach to athermal β→ω transformation. Computational Materials Science, 2012, 53, 187-193.	3.0	21
152	Hydrogenation behavior of high-energy ball milled amorphous Mg2Ni catalyzed by multi-walled carbon nanotubes. International Journal of Hydrogen Energy, 2013, 38, 16168-16176.	7.1	21
153	Non-isothermal synergetic catalytic effect of TiF3 and Nb2O5 on dehydrogenation high-energy ball milled MgH2. Materials Chemistry and Physics, 2016, 183, 65-75.	4.0	21
154	Microstructure and texture evolution of a near β titanium alloy Ti-7333 during continuous cooling hot deformation. Progress in Natural Science: Materials International, 2019, 29, 50-56.	4.4	21
155	Theoretical Calculation and Molecular Design for High Explosives: Theoretical Study on Polynitropyrazines and TheirN-oxides. Propellants, Explosives, Pyrotechnics, 2004, 29, 231-235.	1.6	20
156	On discussion of the applicability of local Avrami exponent: Errors and solutions. Materials Letters, 2009, 63, 1153-1155.	2.6	20
157	Determination of kinetic parameters during isochronal crystallization of Ti40Zr25Ni8Cu9Be18 metallic glass. Journal of Alloys and Compounds, 2009, 479, 835-839.	5.5	20
158	Influences of material parameters on deep drawing of thin-walled hemispheric surface part. Transactions of Nonferrous Metals Society of China, 2009, 19, 433-437.	4.2	20
159	Grain boundary character distribution and texture evolution in cold-drawn Ti–45Nb wires. Materials Letters, 2013, 98, 254-257.	2.6	20
160	Synergetic catalytic effect of MWCNTs and TiF3 on hydrogenation properties of nanocrystalline Mg-10wt%Ni alloys. International Journal of Hydrogen Energy, 2013, 38, 12904-12911.	7.1	20
161	First principles investigation on the stability and elastic properties of Ni2Cr1â^'xMx (MÂ=ÂNb, Mo, Ta, and) Tj ETQ	q110.7	/84314 rgBT 20
162	Structure, composition and morphology of bioactive titanate layer on porous titanium surfaces.	6.1	20

Applied Surface Science, 2014, 308, 1-9.

#	Article	IF	CITATIONS
163	Hot corrosion characteristics of Ni–20Cr–18W superalloy in molten salt. Transactions of Nonferrous Metals Society of China, 2015, 25, 3840-3846.	4.2	20
164	The origin of striation in the metastable β phase of titanium alloys observed by transmission electron microscopy. Journal of Applied Crystallography, 2017, 50, 795-804.	4.5	20
165	The microstructure of NbTi superconducting composite wire for ITER project. Physica C: Superconductivity and Its Applications, 2008, 468, 1840-1842.	1.2	19
166	Dehydrogenation behavior and microstructure evolution of hydrogenated magnesium–nickel–yttrium melt-spun ribbons. RSC Advances, 2015, 5, 54258-54265.	3.6	19
167	Cellular automata simulations of grain growth in the presence of second-phase particles. Modelling and Simulation in Materials Science and Engineering, 2015, 23, 065010.	2.0	19
168	Experimental platform for solidification and <i>in-situ</i> magnetization measurement of undercooled melt under strong magnetic field. Review of Scientific Instruments, 2015, 86, 025102.	1.3	19
169	Indentation Pileup Behavior of Ti-6Al-4V Alloy: Experiments and Nonlocal Crystal Plasticity Finite Element Simulations. Metallurgical and Materials Transactions A: Physical Metallurgy and Materials Science, 2017, 48, 2051-2061.	2.2	19
170	Superplastic deformation mechanism of a γ-TiAl alloy with coarse and bimodal grain structure. Materials Letters, 2017, 194, 58-61.	2.6	19
171	Hot Deformation Behavior, Dynamic Recrystallization, and Texture Evolution of Ti–22Al–25Nb Alloy. Advanced Engineering Materials, 2018, 20, 1700587.	3.5	19
172	Dynamic recrystallization and phase transformation behavior of a wrought β-γ TiAl alloy during hot compression. Progress in Natural Science: Materials International, 2020, 30, 517-525.	4.4	19
173	Strain rate response of a Ti-based metallic glass composite at cryogenic temperature. Materials Letters, 2014, 117, 228-230.	2.6	18
174	Anisotropic porous titanium with superior mechanical compatibility in the range of physiological strain rate for trabecular bone implant applications. Materials Letters, 2014, 137, 424-427.	2.6	18
175	Rheological behavior of Cu–Zr-based metallic glass in the supercooled liquid region. Journal of Alloys and Compounds, 2014, 592, 189-195.	5.5	18
176	Precipitation of nanosized DO22 superlattice with high thermal stability in an Ni–Cr–W superalloy. Scripta Materialia, 2014, 76, 49-52.	5.2	18
177	Magnetic field enhanced phase precipitation in an undercooled Co–Sn alloy. Materials Letters, 2015, 139, 288-291.	2.6	18
178	Hydrogen absorption behavior of Zr-based getter materials with Pd Ag coating against gaseous impurities. International Journal of Hydrogen Energy, 2016, 41, 14778-14787.	7.1	18
179	Strong magnetic field effect on the nucleation of a highly undercooled Co-Sn melt. Scientific Reports, 2017, 7, 4958.	3.3	18
180	Vacuum Tribological Properties of a Ti-46Al-2Cr-2Nb Intermetallics. Journal of Tribology, 2014, 136, .	1.9	17

#	Article	IF	CITATIONS
181	Microstructure Characterization and Mechanical Properties of In Situ Synthesized Ti ₂ <scp>A</scp> l <scp>N</scp> ti48 <scp>A</scp> l2 <scp>C</scp> r2 <scp>N</scp> b Composites. Advanced Engineering Materials, 2014, 16, 507-510.	3.5	17
182	Microstructures and hydrogenation properties of (ZrTi)(V1â^'xAlx)2 Laves phase intermetallic compounds. Journal of Alloys and Compounds, 2015, 645, 358-368.	5.5	17
183	Dendrite size dependence of mechanical properties of in-situ Ti-based bulk metallic glass matrix composites. Materials Science & Engineering A: Structural Materials: Properties, Microstructure and Processing, 2017, 704, 77-81.	5.6	17
184	Insight into solid-solution strengthened bulk and stacking faults properties in Ti alloys: a comprehensive first-principles study. Journal of Materials Science, 2018, 53, 7493-7505.	3.7	17
185	The cavitation of high Nb-containing TiAl alloys during tensile tests around BDTT. Materials Science & Engineering A: Structural Materials: Properties, Microstructure and Processing, 2018, 729, 86-93.	5.6	17
186	A brief review of data-driven ICME for intelligently discovering advanced structural metal materials: Insight into atomic and electronic building blocks. Journal of Materials Research, 2020, 35, 872-889.	2.6	17
187	Hot Deformation and Subsequent Annealing on the Microstructure and Hardness of an Al0.3CoCrFeNi High-entropy Alloy. Acta Metallurgica Sinica (English Letters), 2021, 34, 1527-1536.	2.9	17
188	Design of metastable β-Ti alloys with enhanced mechanical properties by coupling αS precipitation strengthening and TRIP effect. Materials Science & Engineering A: Structural Materials: Properties, Microstructure and Processing, 2022, 835, 142696.	5.6	17
189	An integral fitting method for analyzing the isochronal transformation kinetics: Application to the crystallization of a Ti-based amorphous alloy. Journal of Physics and Chemistry of Solids, 2009, 70, 1448-1453.	4.0	16
190	Microstructure and mechanical properties of new metastable β type titanium alloy. Transactions of Nonferrous Metals Society of China, 2010, 20, 2253-2258.	4.2	16
191	Structural relaxation of Ti40Zr25Ni8Cu9Be18 bulk metallic glass. Journal of Non-Crystalline Solids, 2011, 357, 110-115.	3.1	16
192	In situ investigation on transformation of valence on the surface of the alloy during thermal activation. Solid State Communications, 2011, 151, 842-845.	1.9	16
193	Microstructure and hydrogenation kinetics of Mg2Ni-based alloys with addition of Nd, Zn and Ti. Transactions of Nonferrous Metals Society of China, 2013, 23, 3677-3684.	4.2	16
194	Anomalous magnetism and normal field instability in supercooled liquid cobalt. Applied Physics Letters, 2014, 105, 144101.	3.3	16
195	WidmannstÃ u en laths in Ti48Al2Cr2Nb alloy by undercooled solidification. Materials Characterization, 2015, 107, 156-160.	4.4	16
196	Precipitation behaviors in a quenched high Nb-containing TiAl alloy during annealing. Intermetallics, 2017, 89, 79-85.	3.9	16
197	When a defect is a pathway to improve stability: a case study of the L12 Co3TM superlattice intrinsic stacking fault. Journal of Materials Science, 2019, 54, 13609-13618.	3.7	16
198	The ω phase transformation during the low temperature aging and low rate heating process of metastable \hat{I}^2 titanium alloys. Materials Chemistry and Physics, 2020, 239, 122125.	4.0	16

#	Article	IF	CITATIONS
199	Stress-induced α″ martensitic phase transformation and martensitic twinning in a metastable β titanium alloy. Journal of Alloys and Compounds, 2021, 859, 157809.	5.5	16
200	Microstructural influences on the high cycle fatigue life dispersion and damage mechanism in a metastable β titanium alloy. Journal of Materials Science and Technology, 2021, 70, 12-23.	10.7	16
201	Strengthening efficiency competition between carbon nanotubes (CNTs) and in-situ Al4C3 nanorods in CNTs/Al composites influenced by alumina characteristics. Composites Part A: Applied Science and Manufacturing, 2022, 152, 106704.	7.6	16
202	Numerical Simulation of Titanium Alloy Ingot Solidification Structure during VAR Process Based on Three-Dimensional CAFE Method. Rare Metal Materials and Engineering, 2014, 43, 1537-1542.	0.8	15
203	Microstructure evolution and tensile properties of Ti–6.5Al–2Zr–Mo–V alloy processed with thermo hydrogen treatment. Materials Science & Engineering A: Structural Materials: Properties, Microstructure and Processing, 2014, 619, 274-280.	5.6	15
204	Effect of MWCNTs on hydrogen storage properties of a Zr-based Laves phase alloy. International Journal of Hydrogen Energy, 2016, 41, 4168-4176.	7.1	15
205	Metadynamic recrystallization behavior of β-solidified TiAl alloy during post-annealing after hot deformation. Intermetallics, 2020, 117, 106679.	3.9	15
206	Liquidâ^'liquid structure transition in metallic melt and its impact on solidification: A review. Transactions of Nonferrous Metals Society of China, 2020, 30, 2293-2310.	4.2	15
207	Revealing foundations of the intergranular corrosion of 5XXX and 6XXX Al alloys. Materials Letters, 2020, 271, 127767.	2.6	15
208	Electronic structures and properties of TiAl/Ti2AlNb heterogeneous interfaces: A comprehensive first-principles study. Intermetallics, 2021, 133, 107173.	3.9	15
209	Remarkable cryogenic strengthening and toughening in nano-coherent CoCrFeNiTi0.2 high-entropy alloys via energetically-tuning polymorphous precipitates. Materials Science & Engineering A: Structural Materials: Properties, Microstructure and Processing, 2022, 842, 143111.	5.6	15
210	Non-equilibrium transformation in hypercooled Fe83B17 alloy. Materials Science & Engineering A: Structural Materials: Properties, Microstructure and Processing, 2007, 458, 1-6.	5.6	14
211	Numerical simulation of temperature distribution and heat transfer during solidification of titanium alloy ingots in vacuum arc remelting process. Transactions of Nonferrous Metals Society of China, 2010, 20, 1957-1962.	4.2	14
212	Experimental study of the dissolution and reprecipitation behaviors of ωo phase in high Nb containing TiAl alloy. Materials Characterization, 2015, 109, 122-127.	4.4	14
213	The solidification path related columnar-to-equiaxed transition in Ti–Al alloys. Intermetallics, 2015, 59, 81-86.	3.9	14
214	Surface valence transformation during thermal activation and hydrogenation thermodynamics of Mg–Ni–Y melt-spun ribbons. Applied Surface Science, 2016, 371, 35-43.	6.1	14
215	Hydrogen storage performance of a pseudo-binary Zr-V-Ni Laves phase alloy against gaseous impurities. Renewable Energy, 2017, 103, 786-793.	8.9	14
216	Effect of cooling rate on microstructure evolution of Ti-45Al-8.5Nb-0.2W-0.2B-0.02Y alloy during multi-step heat treatment. Materials Characterization, 2018, 145, 210-217.	4.4	14

#	Article	IF	CITATIONS
217	Intermediate temperature brittleness in a directionally solidified nickel-based superalloy M4706. Materials Science & Engineering A: Structural Materials: Properties, Microstructure and Processing, 2019, 759, 530-536.	5.6	14
218	Tensile properties and deformation micromechanism of Ti-based metallic glass composite containing impurity elements. Journal of Alloys and Compounds, 2019, 784, 220-230.	5.5	14
219	High-throughput investigations of configurational-transformation-dominated serrations in CuZr/Cu nanolaminates. Journal of Materials Science and Technology, 2020, 53, 192-199.	10.7	14
220	The interplay relationship between phase transformation and deformation behavior during hot compression in a metastable β titanium alloy. Materials and Design, 2021, 197, 109275.	7.0	14
221	Formation mechanism of γ twins in β-solidified γ-TiAl alloys. Journal of Materials Science and Technology, 2022, 105, 164-171.	10.7	14
222	Kinetic analysis of the isochronal crystallization of Ti40Zr25Ni8Cu9Be18 metallic glass. Journal of Non-Crystalline Solids, 2009, 355, 420-424.	3.1	13
223	Formation of Ti–Zr–Ni–Cu–Be–Nb bulk metallic glasses. Journal of Alloys and Compounds, 2009, 467, 235-240.	5.5	13
224	Novel configuration of processing bulk textured YB2Cu3O7â^'x superconductor by seeded infiltration growth method. Physica C: Superconductivity and Its Applications, 2010, 470, 68-74.	1.2	13
225	3D finite element simulation of explosive welding of three-layer plates. Science China: Physics, Mechanics and Astronomy, 2011, 54, 890-896.	5.1	13
226	Deformation behavior of a Ti-based bulk metallic glass composite in the supercooled liquid region. Materials and Design, 2016, 90, 595-600.	7.0	13
227	Effect of liquid–liquid structure transition on the nucleation in undercooled Co–Sn eutectic alloy. Materials Chemistry and Physics, 2016, 170, 261-265.	4.0	13
228	Tune the mechanical properties of Ti-based metallic glass composites by additions of nitrogen. Materials Science & Engineering A: Structural Materials: Properties, Microstructure and Processing, 2017, 694, 93-97.	5.6	13
229	Effect of Cold Rolling on the Phase Transformation Kinetics of an Al0.5CoCrFeNi High-Entropy Alloy. Entropy, 2018, 20, 917.	2.2	13
230	The Formation and Evolution of Shear Bands in Plane Strain Compressed Nickel-Base Superalloy. Metals, 2018, 8, 141.	2.3	13
231	Dendrite growth in undercooled Fe–Co melt. Journal of Alloys and Compounds, 2008, 455, L6-L9.	5.5	12
232	Influence of oxygen on microstructure and phase transformation in high Nb containing TiAl alloys. Materials Letters, 2012, 83, 198-201.	2.6	12
233	Hydrogenation properties of Pd-coated Zr-based Laves phase compounds. Vacuum, 2014, 109, 191-196.	3.5	12
234	Overheating dependent undercooling in a hypoeutectic Co–B alloy. Materials Chemistry and Physics, 2015, 149-150, 17-20.	4.0	12

#	Article	IF	CITATIONS
235	Quasi-static and dynamic deformation of an in-situ Ti-based metallic glass composite in supercooled liquid region. Journal of Alloys and Compounds, 2016, 679, 239-246.	5.5	12
236	Characteristics of the Dynamic Recrystallization Behavior of Ti-45Al-8.5Nb-0.2W-0.2B-0.3Y Alloy during High Temperature Deformation. Metals, 2017, 7, 261.	2.3	12
237	Coupling effects of deformation and thermal exposure on the precipitation behaviors of β o (ω) phases in a high Nb-containing TiAl alloy. Materials and Design, 2018, 148, 135-144.	7.0	12
238	Flow behavior and constitutive relationship for elevated temperature compressive deformation of a high Nb containing TiAl alloy with $(\hat{I}\pm 2+\hat{I}^3)$ microstructure. Materials Letters, 2018, 210, 58-61.	2.6	12
239	Mechanical characterization and strain-rate sensitivity measurement of Ti-7333 alloy based on nanoindentation and crystal plasticity modeling. Progress in Natural Science: Materials International, 2018, 28, 718-723.	4.4	12
240	Magnetic-field-induced chain-like assemblies of the primary phase during non-equilibrium solidification of a Co-B eutectic alloy: Experiments and modeling. Journal of Alloys and Compounds, 2020, 815, 152446.	5.5	12
241	An evaluation of nitro derivatives of cubane using ab initio and density functional theories. Theoretical Chemistry Accounts, 2009, 122, 101-106.	1.4	11
242	Investigation on the explosive welding mechanism of corrosion-resisting aluminum and stainless steel tubes through finite element simulation and experiments. International Journal of Minerals, Metallurgy and Materials, 2012, 19, 151-158.	4.9	11
243	Microstructure and Phase Transformation in Ti-22Al-(27-x)Nb-xZr Alloys During Continuous Heating. Journal of Materials Engineering and Performance, 2015, 24, 3951-3957.	2.5	11
244	Reexaminations of the effects of magnetic field on the nucleation of undercooled Cu melt. Japanese Journal of Applied Physics, 2016, 55, 105601.	1.5	11
245	Microstructure and hydrogenation properties of a melt-spun non-stoichiometric Zr-based Laves phase alloy. Materials Characterization, 2016, 111, 53-59.	4.4	11
246	Reversion martensitic phase transformation induced {3Â3Â2}ã€^1Â1Â3〉Âtwinning in metastable β-Ti alloys. Materials Letters, 2020, 272, 127883.	2.6	11
247	Liquid-liquid phase separation in immiscible Cu-Co alloy. Materials Letters, 2020, 268, 127585.	2.6	11
248	Quantitative evaluation of the lamellar kinking&rotation on the flow softening of γ-TiAl-based alloys at elevated temperatures. Materials Letters, 2021, 290, 129458.	2.6	11
249	Crystallography and microstructure of the deformation bands formed in a metastable β titanium alloy during isothermal compression. Materials Characterization, 2021, 176, 111119.	4.4	11
250	Microstructure, phase and microhardness distribution of laser-deposited Ni-based amorphous coating. International Journal of Surface Science and Engineering, 2010, 4, 296.	0.4	10
251	Phase field modeling of isothermal βâ†'ï‰ phase transformation in the Zr–Nb alloys. Computational Materials Science, 2012, 61, 76-82.	3.0	10
252	Interdiffusion in FCC Co-Al-Ti Ternary Alloys. Journal of Phase Equilibria and Diffusion, 2015, 36, 127-135.	1.4	10

#	Article	IF	CITATIONS
253	Evidence for the structure transition in a liquid Co–Sn alloy by in-situ magnetization measurement. Materials Letters, 2015, 145, 261-263.	2.6	10
254	Enhanced mechanical properties of Ti-based metallic glass composites prepared under medium vacuum system. Journal of Non-Crystalline Solids, 2015, 413, 15-19.	3.1	10
255	Hydrogen absorption behavior of a Pd-coated Zr70Fe5.4V24.6 getter material against gaseous impurities. Vacuum, 2015, 122, 222-229.	3.5	10
256	The Effect of Thermal Cycling Treatments on the Thermal Stability and Mechanical Properties of a Ti-Based Bulk Metallic Glass Composite. Metals, 2016, 6, 274.	2.3	10
257	Hydrogen absorption properties of a non-stoichiometric Zr-based Laves alloy againstÂgaseous impurities. International Journal of Hydrogen Energy, 2017, 42, 10109-10116.	7.1	10
258	Microstructure and Crystallography of α Phase Nucleated Dynamically during Thermoâ€Mechanical Treatments in Metastable β Titanium Alloy. Advanced Engineering Materials, 2017, 19, 1600859.	3.5	10
259	Stress relaxation induced spheroidization of the lamellar α phase in Ti-7333 alloy. Journal of Alloys and Compounds, 2019, 781, 674-679.	5.5	10
260	Temperature-induced structure transition in a liquid Co-B eutectic alloy. Materials Letters, 2019, 234, 351-353.	2.6	10
261	The effect of cubic-texture on fatigue cracking in a metastable Î ² titanium alloy subjected to high-cycle fatigue. International Journal of Fatigue, 2020, 141, 105872.	5.7	10
262	Microstructure and properties of AlCoCrCuFeNi high-entropy alloy solidified under high magnetic field. Materials Letters, 2021, 285, 129182.	2.6	10
263	Experimental and simulation analysis of residual topography dominated deformation mechanism of nanoindentation: a case study of Inconel 625 superalloy. Journal of Materials Research and Technology, 2021, 13, 1521-1533.	5.8	10
264	Microstructural sensitivity and deformation micro-mechanisms of a bimodal metastable β titanium Ti–7Mo–3Nb–3Cr–3Al alloy. Materials Science & Engineering A: Structural Materials: Properties, Microstructure and Processing, 2021, 824, 141821.	5.6	10
265	Heterogeneous precipitate microstructure in titanium alloys for simultaneous improvement of strength and ductility. Journal of Materials Science and Technology, 2022, 124, 150-163.	10.7	10
266	A facile synthesis and the asymmetric catalytic activity of BINOL-based thiazole (thiadiazole) thioether ligands. Journal of Organometallic Chemistry, 2008, 693, 17-22.	1.8	9
267	Effects of Nb on the formation of icosahedral quasicrystalline phase in Ti-rich Ti–Zr–Ni–Cu–Be glassy forming alloys. Journal of Non-Crystalline Solids, 2008, 354, 3332-3335.	3.1	9
268	Effects of Zn addition on the improvement of glass forming ability and plasticity of Mg–Cu–Tb bulk metallic glasses. Journal of Non-Crystalline Solids, 2008, 354, 5368-5371.	3.1	9
269	Computational study of atomic mobility for the bcc phase of the U–Pu–Zr ternary system. Journal of Nuclear Materials, 2010, 407, 220-227.	2.7	9
270	Crystallization and compressive behaviors of Ti40Zr25Ni8Cu9Be18 BMG cast from different liquid states. Intermetallics, 2012, 28, 45-50.	3.9	9

#	Article	IF	CITATIONS
271	Microstructure evolution and nitrides precipitation in in-situ Ti2AIN/TiAl composites during isothermal aging at 900 °C. Transactions of Nonferrous Metals Society of China, 2014, 24, 1372-1378.	4.2	9
272	Poisoning effect of oxygen on hydrogenation performance of a Zr-V-Ni Laves phase alloy. International Journal of Hydrogen Energy, 2016, 41, 19114-19122.	7.1	9
273	Microstructure Evolution during Cold-Deformation and Aging Response after Annealing of TB8 Titanium Alloy. Rare Metal Materials and Engineering, 2016, 45, 575-580.	0.8	9
274	Instability Pattern Formation in a Liquid Metal under High Magnetic Fields. Scientific Reports, 2017, 7, 2248.	3.3	9
275	Effect of Solidification on Microstructure and Properties of FeCoNi(AlSi)0.2 High-Entropy Alloy Under Strong Static Magnetic Field. Entropy, 2018, 20, 275.	2.2	9
276	The effect of high magnetic field on the microstructure evolution of a Cu-Co alloy during non-equilibrium solidification. Journal of Crystal Growth, 2019, 515, 78-82.	1.5	9
277	Effect of strain distribution on the evolution of $\hat{I}\pm$ phase and texture for dual-phase titanium alloy during multi-pass forging process. Materials Chemistry and Physics, 2019, 228, 318-324.	4.0	9
278	Stress relaxation induced morphological evolution and texture weakening of α phase in Ti-6Al-4V alloy. Materials Letters, 2019, 236, 148-151.	2.6	9
279	Heat Treatment Influence on Tribological Properties of AlCoCrCuFeNi High-Entropy Alloy in Hydrogen Peroxide-Solution. Metals and Materials International, 2020, 26, 1286-1294.	3.4	9
280	Combined crystal plasticity simulations and experiments for parameter identification: application to near-l ² titanium alloy. Journal of Materials Science, 2020, 55, 15043-15055.	3.7	9
281	Outstanding self-lubrication of SiC ceramic with porous surface/AlCoCrFeNiTi0.5 high-entropy alloy tribol-pair under 90Âwt% H2O2 harsh environment. Materials Letters, 2020, 276, 128025.	2.6	9
282	Effects of microstructure on high cycle fatigue properties of dual-phase Ti alloy: combined nonlocal CPFE simulations and extreme value statistics. Journal of Materials Research and Technology, 2020, 9, 5991-6000.	5.8	9
283	A novel trinuclear titanium(IV) complex with a C3 axis along Ti1–Ti2–Ti3 containing 3-[(1H-1,2,4-triazol-1-yl)methyl]-BINOLate ligands: synthesis, structure, and reactivity. Tetrahedron: Asymmetry, 2006, 17, 2149-2153.	1.8	8
284	Assessment of the atomic mobilities for ternary Al–Cu–Zn fcc alloys. Calphad: Computer Coupling of Phase Diagrams and Thermochemistry, 2010, 34, 68-74.	1.6	8
285	Nanocrystallization-induced large room-temperature compressive plastic strain of Ti40Zr25Ni8Cu9Be18 BMG. Journal of Alloys and Compounds, 2011, 509, 1626-1629.	5.5	8
286	Study on tribological properties of ceramics/stainless steel rubbing pairs in hydrogen peroxide solutions. Wear, 2011, 271, 1617-1622.	3.1	8
287	Coherent elastic energy calculation of ï‰ particles in β matrix for Zr–Nb alloys. Journal of Materials Science, 2011, 46, 675-680.	3.7	8
288	Effect of Nb Content on Solidification Characteristics and Microsegregation in Cast Ti–48Al–xNb Alloys. Acta Metallurgica Sinica (English Letters), 2016, 29, 714-721.	2.9	8

#	Article	IF	CITATIONS
289	Optimization of thermal processing parameters of Ti555211 alloy using processing maps based on Murty criterion. Rare Metals, 2016, 35, 154-161.	7.1	8
290	Deformation behaviors of a Ti-based bulk metallic glass composite in the dendrite softening region. Materials Science & Engineering A: Structural Materials: Properties, Microstructure and Processing, 2016, 653, 1-7.	5.6	8
291	Precipitation behavior of α2 phase in Ti–34Al–13Nb alloy. Journal of Alloys and Compounds, 2017, 725, 155-162.	5.5	8
292	Flow characteristics and deformation mechanisms for TiAl/Ti2AlNb diffusion bonded joint. Materials Chemistry and Physics, 2018, 220, 216-224.	4.0	8
293	A novel strategy for enhancing mechanical performance of Al0.5CoCrFeNi high-entropy alloy via high magnetic field. Materials Letters, 2019, 240, 250-252.	2.6	8
294	Composition dependent characteristic transition temperatures of Co-B melts. Journal of Non-Crystalline Solids, 2019, 522, 119583.	3.1	8
295	Interstitial triggered grain boundary embrittlement of Al–X (X = H, N and O). Computational Materials Science, 2019, 163, 241-247.	3.0	8
296	Mechanical properties and microstructure of in situ formed Ti2AlN/TiAl(WMS) composites. Rare Metals, 2021, 40, 190-194.	7.1	8
297	Thermal–Mechanical Processing and Strengthen in AlxCoCrFeNi High-Entropy Alloys. Frontiers in Materials, 2021, 7, .	2.4	8
298	Hot tensile behavior of a TiAl alloy with a (βO +Âγ) microduplex microstructure prepared simply by heat treatments. Journal of Alloys and Compounds, 2021, 875, 160039.	5.5	8
299	Enhanced mechanical properties of a metastable β titanium alloy via optimized thermomechanical processing. Materials Science & Engineering A: Structural Materials: Properties, Microstructure and Processing, 2022, 840, 142997.	5.6	8
300	Dual-frequency electromagnetic confinement of liquid aluminum. Journal of Materials Processing Technology, 2005, 166, 449-454.	6.3	7
301	Synthesis of modified H4-BINOL ligands and their applications in the asymmetric addition of diethylzinc to aromatic aldehydes. Tetrahedron: Asymmetry, 2006, 17, 1842-1845.	1.8	7
302	3â€Substituted BINOL Schiff bases and their reductive products for catalytic asymmetric addition of diethylzinc to aldehydes. Chirality, 2008, 20, 828-832.	2.6	7
303	Effects of stress state on texture and microstructure in cold drawing-bulging of CP-Ti sheet. Transactions of Nonferrous Metals Society of China, 2013, 23, 23-31.	4.2	7
304	Precipitation Behavior of Pt2Mo-Type Superlattices in Hastelloy C-2000 Superalloy with Low Mo/Cr Ratio. Journal of Materials Engineering and Performance, 2014, 23, 3314-3320.	2.5	7
305	Formation mechanism of tetrahedral MgYNi4 phase. Materials Letters, 2015, 145, 193-196.	2.6	7
306	Temperature dependent dynamic flow behavior of an in-situ Ti-based bulk metallic glass composite. Materials Science & Engineering A: Structural Materials: Properties, Microstructure and Processing, 2015, 627, 21-26.	5.6	7

#	Article	IF	CITATIONS
307	Effects of subgrain size and static recrystallization on the mechanical performance of polycrystalline material: A microstructure-based crystal plasticity finite element analysis. Progress in Natural Science: Materials International, 2015, 25, 58-65.	4.4	7
308	Characterization of Hot Deformation Behavior of a New Near-Î ² Titanium Alloy: Ti555211. High Temperature Materials and Processes, 2016, 35, 913-928.	1.4	7
309	Dry-sliding tribological properties of AlCoCrFeNiTi0.5 high-entropy alloy. Rare Metals, 2022, 41, 4266-4272.	7.1	7
310	Simulation of Intergranular Ductile Cracking in Î ² Titanium Alloys Based on a Micro-Mechanical Damage Model. Materials, 2017, 10, 1250.	2.9	7
311	Microplasticity behavior study of equiaxed near-β titanium alloy under high-cycle fatigue loading: crystal plasticity simulations and experiments. Journal of Materials Research and Technology, 2019, 8, 6146-6157.	5.8	7
312	Pitting Corrosion of Natural Aged Al–Mg–Si Extrusion Profile. Materials, 2019, 12, 1081.	2.9	7
313	Thermally-induced α→β phase transformation interweaving with abnormal α grain growth in hot extruded TNM alloy. Journal of Materials Research and Technology, 2021, 15, 2036-2044.	5.8	7
314	Quasi-in-situ investigation on microstructure degradation of a fully lamellar TiAl alloy during creep. Journal of Materials Research and Technology, 2022, 18, 4980-4989.	5.8	7
315	Finite element simulation on the deep drawing of titanium thin-walled surface part. Rare Metals, 2010, 29, 108-113.	7.1	6
316	Macrosegregation Behavior of Ti-10V-2Fe-3Al Alloy During Vacuum Consumable Arc Remelting Process. Journal of Materials Engineering and Performance, 2011, 20, 65-70.	2.5	6
317	Oxidation behavior of Hastelloy C-2000 superalloy at 800 °C and 1000 °C. Transactions of Nonferrous Metals Society of China, 2015, 25, 354-362.	4.2	6
318	Microstructure evolution of a new near- \hat{l}^2 titanium alloy: Ti555211 during high-temperature deformation. Rare Metals, 2015, 34, 757-763.	7.1	6
319	A Twoâ€Step Heat Treatment to Eliminate the Microâ€Segregation of Ti–45Al–8.5Nb–0.2W–0.2B–0. Alloy. Advanced Engineering Materials, 2016, 18, 1267-1272.	02Y 3.5	6
320	Evolution behavior of superlattice phase with Pt ₂ Mo-type structure in Ni–Cr–Mo alloy with low atomic Mo/Cr ratio. Journal of Materials Research, 2016, 31, 427-434.	2.6	6
321	Hot corrosion behavior and mechanical properties degradation of a Ni–Cr–W-based superalloy. Rare Metals, 2017, 36, 23-31.	7.1	6
322	A new microscopic coordinated deformation model of Ti-based bulk metallic composites during tensile deformation. Scripta Materialia, 2019, 172, 23-27.	5.2	6
323	Solidification of Immiscible Alloys under High Magnetic Field: A Review. Metals, 2021, 11, 525.	2.3	6
324	Effects of an ultra-high magnetic field up to 25 T on the phase transformations of undercooled Co-B eutectic alloy. Journal of Materials Science and Technology, 2021, 93, 79-88.	10.7	6

#	Article	IF	CITATIONS
325	Experiments and crystal plasticity simulations for the deformation behavior of nanoindentation: Application to the 1±2 phase of TiAl alloy. Materials Science & Engineering A: Structural Materials: Properties, Microstructure and Processing, 2021, 831, 142283.	5.6	6
326	Effect of melt heat treatment on the solid/liquid interface morphology of directional solidification. Science and Technology of Advanced Materials, 2001, 2, 169-172.	6.1	5
327	Interface morphology evolvement and microstructure characteristics of hypoeutectic Cu–1.0 wt%Cr alloy during unidirectional solidification. Science and Technology of Advanced Materials, 2005, 6, 950-955.	6.1	5
328	On the tension necking of copper single crystal specimen under slip deformation mechanism. Science in China Series D: Earth Sciences, 2007, 50, 308-318.	0.9	5
329	Deviations from the classical Johnson–Mehl–Avrami kinetics. Journal of Alloys and Compounds, 2008, 460, 326-330.	5.5	5
330	Interfacial characteristics and dynamic mechanical properties of Wf/Zr-based metallic glass matrix composites. Transactions of Nonferrous Metals Society of China, 2008, 18, 77-81.	4.2	5
331	Microstructure evolution in undercooled Co80Pd20 alloys. Journal of Materials Science, 2011, 46, 5495-5502.	3.7	5
332	Effect of remelting current on molten pool profile of titanium alloy ingot during vacuum arc remelting process. Journal of Shanghai Jiaotong University (Science), 2011, 16, 133-136.	0.9	5
333	Effect of strain rate on impact response and ï‰ transformation of quenched Zr–Nb alloys. Materials Characterization, 2013, 84, 10-15.	4.4	5
334	Computational diffusion kinetics and its applications in study and design of rare metallic materials. Science Bulletin, 2014, 59, 1672-1683.	1.7	5
335	Thermal Stability and the Matrix Induced Brittleness in a Ti-based Bulk Metallic Glass Composite. Materials Research, 2015, 18, 83-88.	1.3	5
336	Effects of hot compression on carbide precipitation behavior of Ni—20Cr—18W—1Mo superalloy. Transactions of Nonferrous Metals Society of China, 2016, 26, 2883-2891.	4.2	5
337	Ordering Transformation and Age Hardening in a Ni-Cr-W Superalloy. Metallurgical and Materials Transactions A: Physical Metallurgy and Materials Science, 2016, 47, 5907-5917.	2.2	5
338	Precipitation of coherent Ni2(Cr, W) superlattice in an Ni–Cr–W superalloy. Materials Characterization, 2016, 111, 86-92.	4.4	5
339	Reply to comments on "composite structure of α phase in metastable β Ti alloys induced by lattice strain during β to α phase transformation―by prof. D. Banerjee. Scripta Materialia, 2017, 141, 148-150.	5.2	5
340	Microstructure Evolution of a High Nb Containing TiAl Alloy with (α2 + γ) Microstructure during Elevated Temperature Deformation. Metals, 2018, 8, 916.	2.3	5
341	Microstructural evolution and tensile properties of an in-situ TiZr-based bulk metallic glass matrix composite after hot-pressing deformation in its supercooled liquid region. Journal of Alloys and Compounds, 2018, 768, 415-424.	5.5	5
342	Influence of Isothermal ï‰ Transitional Phase-Assisted Phase Transition From β to α on Room-Temperature Mechanical Performance of a Meta-Stable β Titanium Alloy Tiâ^'10Moâ^'6Zrâ^'4Snâ^'3Nb (Ti-B12) for Medical Application. Frontiers in Bioengineering and Biotechnology, 2020, 8, 626665.	4.1	5

#	Article	IF	CITATIONS
343	A facile synthesis and asymmetric catalytic activity of new 3â€substituted chiral BINOL ligands. Applied Organometallic Chemistry, 2008, 22, 55-58.	3.5	4
344	Microstructure and stopped growth mechanism of Y123 bulk fabricated by directional infiltration and growth. Transactions of Nonferrous Metals Society of China, 2008, 18, 1139-1144.	4.2	4
345	Limitation of the Johnson-Mehl-Avrami equation for the kinetic analysis of crystallization in a Ti-based amorphous alloy. International Journal of Minerals, Metallurgy and Materials, 2010, 17, 307-311.	4.9	4
346	Mechanism of seeded infiltration growth process analysed by magnetic susceptibility measurements and in situ observation. Ceramics International, 2010, 36, 1383-1388.	4.8	4
347	Behavior of oxygen diffusion in buffer layers for coated conductors. Journal of Alloys and Compounds, 2011, 509, 8812-8824.	5.5	4
348	Corrosion Behavior of Ni–20Cr–18W–1Mo Superalloy in Supercritical Water. Acta Metallurgica Sinica (English Letters), 2014, 27, 1046-1056.	2.9	4
349	Structure transitions near liquidus and the nucleation of undercooled melt of Ni–Cr–W superalloy. Physica B: Condensed Matter, 2014, 454, 8-14.	2.7	4
350	Effect of α′ Martensite on Microstructure Refinement After αÂ+Âβ Isothermal Treatment in a Near-α Titanium Alloy Ti60. Journal of Materials Engineering and Performance, 2015, 24, 1945-1952.	¹ 2.5	4
351	Phase Transformation Kinetics of a FCC Al0.25CoCrFeNi High-Entropy Alloy during Isochronal Heating. Metals, 2018, 8, 1015.	2.3	4
352	Microstructure and Hydrogen Absorption Properties of a BCC Phase Accompanied Laves Alloy. Metals and Materials International, 2019, 25, 814-820.	3.4	4
353	PHASE SELECTION AND THE SOLIDIFICATION CHARACTERISTICS OF TIAl BASE ALLOYS IN THE NONEQUILIBRIUM SOLIDIFICATION. Jinshu Xuebao/Acta Metallurgica Sinica, 2013, 49, 1295.	0.3	4
354	Microstructure Characterization and Thermal Stability of TNM Alloy Fabricated by Powder Hot Isostatic Pressing. Metals, 2021, 11, 1720.	2.3	4
355	Revealing sulfur- and phosphorus-induced embrittlement and local structural phase transformation of superlattice intrinsic stacking faults in L12-Ni3Al. Journal of Materials Science, 2022, 57, 12483-12496.	3.7	4
356	Effects of Ta addition on the microstructure and mechanical properties of Ti40Zr25Ni8Cu9Be18 amorphous alloy. International Journal of Minerals, Metallurgy, and Materials, 2007, 14, 31-35.	0.2	3
357	Enhancing magnetic properties of anisotropic NdDyFeCoNbCuB powder by applying magnetic field at high temperature during hydrogen desorption. Rare Metals, 2010, 29, 480-485.	7.1	3
358	First-principles prediction of ductility in β-type Ti-Mo binary alloys. Journal of Shanghai Jiaotong University (Science), 2011, 16, 227-230.	0.9	3
359	Precipitation Behavior of Ï f -FeCr Phases in Hastelloy C-2000 Superalloy Under Plastic Deformation and Aging Treatment. Journal of Materials Engineering and Performance, 2015, 24, 565-571.	2.5	3
360	Dynamic mechanical properties of a Ti-based metallic glass matrix composite. Journal of Applied Physics, 2015, 117, 155102.	2.5	3

#	Article	IF	CITATIONS
361	Tribological Behavior of 1Cr18Ni9Ti Steel under Hydrogen Peroxide Solution against Different Ceramic Counterparts. Rare Metal Materials and Engineering, 2016, 45, 593-598.	0.8	3
362	Hot Workability and Superplasticity of Low-Al and High-Nb Containing TiAl Alloys. Jom, 2017, 69, 2610-2614.	1.9	3
363	Microstructural evolution resulting from different deformation mechanisms of a high-Nb-containing TiAl alloy with harmonic structure during elevated-temperature deformation. Materials Letters, 2019, 242, 35-38.	2.6	3
364	Hot deformation behaviors of WE71 alloy under plain strain compression at elevated temperature. Progress in Natural Science: Materials International, 2020, 30, 526-532.	4.4	3
365	The cryogenic mechanical property deviation of Ti-based bulk metallic glass composite induced by interstitial element. Journal of Non-Crystalline Solids, 2020, 542, 120105.	3.1	3
366	Effect of High Strain Rate on Adiabatic Shearing of $\hat{I}\pm+\hat{I}^2$ Dual-Phase Ti Alloy. Materials, 2021, 14, 2044.	2.9	3
367	Liquid state dependent solidification of a Co-B eutectic alloy under a high magnetic field. Journal of Materials Science and Technology, 2022, 116, 58-71.	10.7	3
368	Research on the dual-frequency electromagnetic shaping of liquid metal. Journal of Materials Processing Technology, 2003, 137, 204-207.	6.3	2
369	Research on the non-linear temperature field of molten metal shaped by an electromagnetic field in DS processing. Journal of Materials Processing Technology, 2003, 137, 145-150.	6.3	2
370	Effect of the kinetic model on parameter distortions in non-isothermal transformations. Journal of Alloys and Compounds, 2009, 479, L22-L25.	5.5	2
371	Modeling of Incommensurate ω Structure in the Zr-Nb Alloys. Metallurgical and Materials Transactions A: Physical Metallurgy and Materials Science, 2012, 43, 2581-2586.	2.2	2
372	Effect of magnetic order on nucleation in undercooled Co80Pd20 melts. Applied Physics Letters, 2013, 102, 022403.	3.3	2
373	Effect of hot-forging on beta phase transformation of a high niobium containing titanium aluminide alloy. International Journal of Modern Physics B, 2015, 29, 1540009.	2.0	2
374	In situ Observation of the Initial Stage of <i>γ</i> Lamella Formation in Ti48Al2Cr2Nb Alloy. Advanced Engineering Materials, 2017, 19, 1600670.	3.5	2
375	Microstructure Evolution of a Ti-45Al-8.5Nb-0.2W-0.2B-0.02Y Alloy during Massive Transformation and Subsequent Annealing. Metals, 2018, 8, 89.	2.3	2
376	Hot Deformation Behavior of a Novel Near-β Titanium Alloy Ti-5.5Mo-6V-7Cr-4Al-2Sn-1Fe in (α+β) Phase Region. Frontiers in Materials, 2020, 6, .	2.4	2
377	The α2 precipitation from equiaxed γ phase in as-cast Ti-44Al-4Nb-2Cr-0.1B alloy. Materials Letters, 2021, 284, 128978.	2.6	2
378	Site Occupation and Structural Phase Transformation of the (010) Antiphase Boundary in Boron-Modified L12 Ni3Al. Jom, 2021, 73, 2285-2292.	1.9	2

#	Article	IF	CITATIONS
379	Revealing the Local Microstates of Fe–Mn–Al Medium Entropy Alloy: A Comprehensive First-principles Study. Acta Metallurgica Sinica (English Letters), 2021, 34, 1492-1502.	2.9	2
380	Precipitation Behavior and Microstructural Evolution of α Phase during Hot Deformation in a Novel β-Air-Cooled Metastable β-Type Ti-B12 Alloy. Metals, 2022, 12, 770.	2.3	2
381	Formation of core-shell structure in immiscible CoCrCuFe1.5Ni0.5 high-entropy alloy. Materials Letters, 2022, , 132452.	2.6	2
382	Effects of 5%Ni addition on thermal stability and crystallization behavior of Mg65Cu25Tb10 bulk metallic glass. Transactions of Nonferrous Metals Society of China, 2008, 18, 1107-1111.	4.2	1
383	Hydrogen absorption of NdDyFeCoNbCuB sintered magnets. Journal of Rare Earths, 2009, 27, 520-524.	4.8	1
384	Deposition of Fe-based metallic glass coatings by Air Plasma Spraying process. International Journal of Surface Science and Engineering, 2010, 4, 288.	0.4	1
385	Enthalpy recovery and its effect on homogeneous flow stress during supercooled liquid region for Ti40Zr25Ni8Cu9Be18 bulk metallic glass. Journal of Non-Crystalline Solids, 2011, 357, 3049-3052.	3.1	1
386	Numerical simulation of fluid flow caused by buoyancy forces during vacuum arc remelting process. Journal of Shanghai Jiaotong University (Science), 2011, 16, 272-276.	0.9	1
387	Multifilamentary MgB2 wires fracture behavior during the drawing process. Physica C: Superconductivity and Its Applications, 2012, 483, 17-20.	1.2	1
388	Diffusion Bonding of Fe-Based Amorphous Ribbon to Crystalline Cu. Materials Science Forum, 2013, 745-746, 788-792.	0.3	1
389	The Localized Corrosion and Stress Corrosion Cracking of a 6005A-T6 Extrusion Profile. Materials, 2021, 14, 4924.	2.9	1
390	Post-bonded compressive behavior and processing map of TiAl/Ti2AlNb joint along the bonding interface based on a composite model. Materials Chemistry and Physics, 2021, 271, 124915.	4.0	1
391	EFFECT OF OXYGEN ON MICROSTRUCTURE AND PHASE TRANSFORMATION OF HIGH Nb CONTAINING TIAl ALLOYS. Jinshu Xuebao/Acta Metallurgica Sinica, 2013, 49, 1381.	0.3	1
392	Analysis on the interface stability and morphology evolution rules of the YBCO crystal growth during the unidirectional solidification. Journal of Alloys and Compounds, 2008, 462, 428-431.	5.5	0
393	Numerical analysis of material properties in deformation of near hemispherical shells. Journal of Shanghai Jiaotong University (Science), 2011, 16, 209-213.	0.9	0
394	Asymmetric deformation of near hemispherical diaphragm under uniform surface load. Journal of Shanghai Jiaotong University (Science), 2011, 16, 214-218.	0.9	0
395	The Nanocrystal and Its Thermal Stability in Ti ₄₀ Zr ₂₅ Ni ₈ Cu ₉ Be ₁₈ Metallic Glass during Homogeneous Deformation. Materials Science Forum, 2011, 688, 431-436.	0.3	0
396	Quantitative phase field simulation of athermal Ї‰ transition in Ti-Mo alloys. , 2013, , 2757-2764.		0

23

#	Article	F	CITATIONS
397	Effects of β-Dendrite Growth Velocity on βÂ→Âα Transformation of Hypoperitectic Ti–46Al–7Nb Alloy. Acta Metallurgica Sinica (English Letters), 2015, 28, 58-63.	2.9	0